Straightforward synthesis of silicon vacancy (SiV) center-containing single-digit nanometer nanodiamonds via detonation process

Yuto Makino [a,b,*,1], Tomoaki Mahiko [a,1], Ming Liu [a], Akihiko Tsurui [a], Taro Yoshikawa [a], Shinji Nagamachi [c], Shigeru Tanaka [d], Kazuyuki Hokamoto [d], Masaaki Ashida [b], Masanori Fujiwara [e], Norikazu Mizuochi [e], Masahiro Nishikawa [a]

[a] *Daicel Corporation, 1239, Shinzaike, Aboshi-ku, Himeji, Hyogo 671-1283, Japan*
[b] *Graduate School of Engineering Science, Osaka University, 1-3, Machikaneyama, Toyonaka, Osaka 560-8531, Japan*
[c] *Nagamachi Science Laboratory, Co., Ltd., 1-16-1-1003, Shioe, Amagasaki, Hyogo 661-0976, Japan*
[d] *Institute of Industrial Nanomaterials, Kumamoto University, 2-39-1, Kurokami, Chuo-ku, Kumamoto-shi, Kumamoto 860-8555, Japan*
[e] *Institute for Chemical Research, Kyoto University, Gokasho, Uji, Kyoto 611-0011, Japan*

ARTICLE INFO

ABSTRACT

Silicon vacancy (SiV) color centers in diamond have attracted widespread attention owing to their stable photoluminescence (PL) with a sharp emission band in the near-infrared region (ZPL 738 nm). Especially, SiV center containing single-digit nanometer-sized nanodiamonds (single-digit SiV-NDs) are desirable for various applications such as bioimaging and biosensing because of their extremely small size, comparable to many biomaterials. Therefore, several attempts have been made to fabricate the single-digit SiV-NDs. However, there are no reports on the successful fabrication of such materials in reasonable scale of production. Here, we report the successful synthesis of single-digit SiV-NDs via straightforward detonation process, which is known to have the high productivity in fabrication of single-digit NDs. Triphenylsilanol (TPS), as a silicon source, was mixed with explosives (TPS/TNT/RDX = 1/59/40 wt%) and the detonation process was carried out. The obtained single-digit NDs exhibit PL at approximately 738 nm, indicating that single-digit SiV-NDs were successfully synthesized. Moreover, we conjectured that the physics behind this achievement may be attributed to the aromatic ring of TPS under the consideration of ND formation mechanism newly built up based on the results of time-resolved optical emission measurements for the detonation reaction.

1. Introduction

Nanodiamonds (NDs) are attractive carbon materials that have both the unique properties of nanoparticles such as a high specific surface area and the prominent physical and chemical properties of bulk diamond [1]. Numerous methods for synthesizing NDs have been studied and developed thus far: chemical vapor deposition (CVD), high-pressure high-temperature (HPHT), and detonation processes are well known [2]. Among these, the detonation process, which produces NDs through detonation of explosives such as a mixture of 2,4,6-trinitrotoluene (TNT) and hexahydro-1,3,5-trinitro-1,3,5-triazine (RDX) [1,2], is advantageous for the following reasons. First, the detonation process exhibits high productivity. The simplicity of the process enables the production of detonation nanodiamonds (DNDs) in large quantities (tens or

hundreds of tons per year) at low cost [3]. Second, DNDs are advantageous over other NDs because their primary particles are uniform, small (4–5 nm), and spherical [1,4]. Moreover, DNDs have surfaces which are freely functionalized [5–7], enabling modification with chemical compounds and dispersion in various media [8–10]. Meanwhile, it should be noted here that DNDs generally contain more sp^2-carbon on the surface than larger particles fabricated by other methods and this can be, in some cases, deleterious for color center charge states.

Due to the aforementioned properties, DNDs have been extensively studied in various applications [2,11,12]. The interest in medical applications of DNDs stems from their size, biocompatibility, and surface functional groups [13,14]. Their small particle size enables DNDs to move into living cells through the membrane [15], and their surface functional groups enable further functionalization with a wide variety of

molecules such as drugs to be delivered into the cell [16–19]. Moreover, attempts have been made to add fluorescence properties to DNDs for bioimaging [20]. In particular, the incorporation of color centers into the diamond lattice has attracted great interest. Quite a few researchers have focused on introducing nitrogen vacancy (NV) centers. They use the nitrogen atoms derived from explosives [14,21–25], some of which are spontaneously incorporated into DNDs and small portion of those atoms can form the substitutional defects. However, NV centers have a disadvantage for bioimaging: their zero-phonon line (ZPL) at 637 nm is outside the near-infrared biological window (650–950 nm) [26,27]. Near-infrared light is absolutely necessary for bioimaging applications as it is hardly absorbed by living tissues and differs from the wavelength range of the autofluorescence of tissues [28–30]. For this reason, incorporation of color centers other than NVs into DNDs is currently desired for the cutting-edge bioimaging techniques. Among more than 500 types of diamond color centers that have been discovered [31], the most anticipated one is the silicon vacancy (SiV) center, schematically illustrated in Fig. 1. SiV centers exhibit stable and non-blinking photoluminescence (PL) with a sharp emission band in the near-infrared region (ZPL at 738 nm) which can be excited by near-infrared light [32–35]. In addition, SiV centers can be activated even in smaller NDs compared to NV centers. The smallest size of diamond that can hold stable color centers is reported to be 24 nm for NV and 8 nm for SiV [36]. Another report, in an ultimate case, states that SiV center is stable even in 1.6 nm-sized NDs [37]. The color centers that are stable in extremely small NDs, such as DNDs, should be suitable for biomarker applications [36].

Not limited to the detonation method, several attempts have been made to fabricate SiV center-containing NDs (SiV-NDs) [26,29,34,38]. However, there are no reports on the successful fabrication of such materials with a particle size of a single-digit nanometer in a reasonable scale of industrial production. In the case of detonation process, SiV centers have never been found in *as-synthesized* DNDs after a lot of trials

in silicon doping within the detonation reaction and, thus, the detonation process itself has been regarded as unpromising for the synthesis of SiV-NDs [1]. In the present study, we challenged the straightforward fabrication of SiV-DNDs with a particle size of a single-digit nanometer via detonation process and succeeded in it using triphenylsilanol (TPS) as a silicon source. Furthermore, the physics behind the successful fabrication of SiV-DNDs using such a silicon dopant (Si-dopant) was discussed from the point of view for the mechanism of DND formation, revealed from the time-resolved optical emission measurements of the detonation phenomena.

2. Experimental procedures

For the standard (undoped) DNDs production, a mixed explosive consisted of 60 wt% TNT and 40 wt% RDX was prepared by compression to form a cylindrical charge of 60 g as the total mass (hereinafter referred to as "TR-explosive"). For the SiV-DNDs synthesis, a certain mass of Si-dopant was added in the course of the aforementioned explosive preparation (hereinafter referred to as "Si-explosive"). In this study, TPS (Tokyo Chemical Industry Co., Ltd.) and tetrakis(trimethylsilyl)silane (TTS) (Tokyo Chemical Industry Co., Ltd.), whose chemical structures are shown in Fig. 2, were chosen as Si-dopants. Those Si-dopants are powdery solid at ambient temperatures and pressures (the melting points of TPS and TTS are 152–154 °C [39] and 263–264 °C [40], respectively), which can, therefore, be mixed with TNT and RDX powders well and then molded by pressing to form the cylindrical shape. The grain size of each powder was adjusted to be below 1 mm.

In the SiV-DNDs synthesis, the two types of Si-explosives, containing 0.6 g of each Si-dopant, were detonated under a CO_2 atmosphere. The detonation product was purified with mixed acid (H_2SO_4 + HNO_3) at 150 °C for 5 h. The reaction mixture was added deionized (DI) water at 70 °C and heated (150 °C) again for 5 h. The precipitate was then rinsed
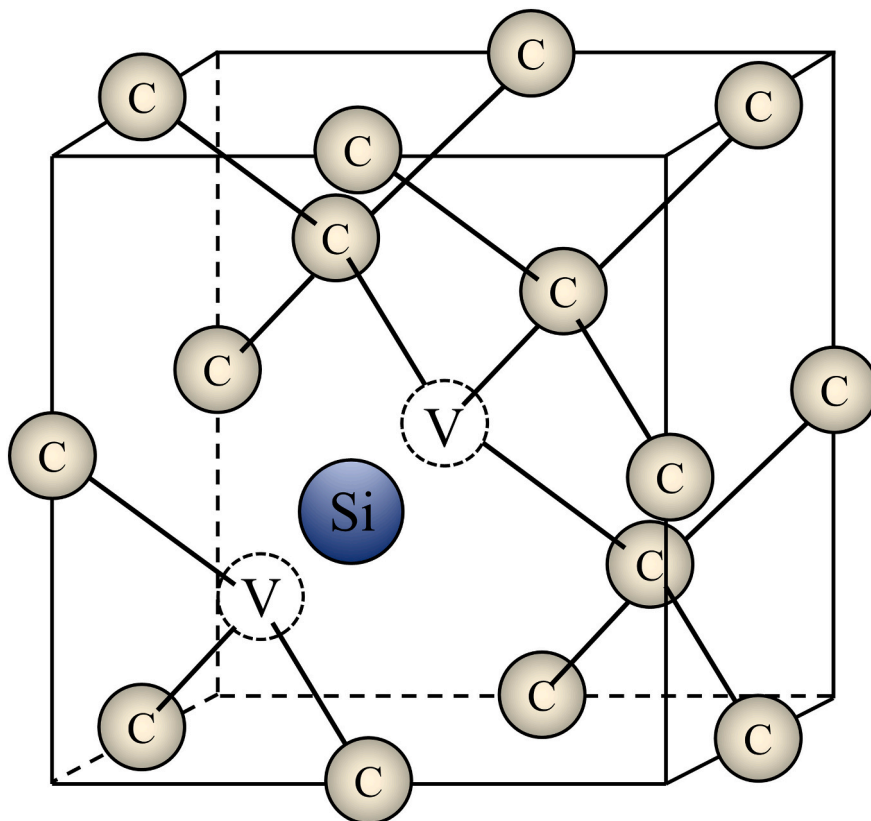

Fig. 1. Structure of the SiV center with a silicon atom in a split vacancy site.
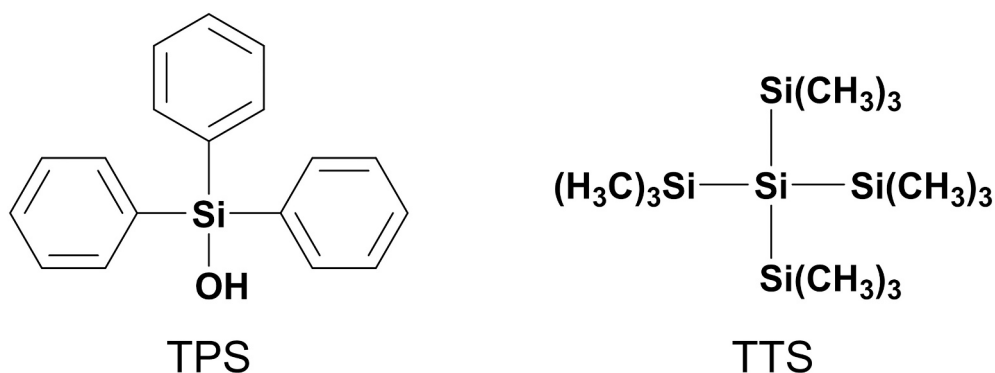
Fig. 2. Chemical structure of the Si-dopants: triphenylsilanol (TPS) and tetrakis(trimethylsilyl)silane (TTS).

with DI water. After drying, the crude product was treated with aqueous 8 M NaOH at 70 °C for 8 h, rinsed with DI water, and dried. Finally, the sample was air-oxidized in O_2/N_2 (4:96 vol%) at 470 °C for 2 h. The sample just after treated with aqueous NaOH was characterized by powder X-ray diffraction (XRD) (Rigaku, SmartLab) analysis with Cu-Kα_1 radiation (λ=1.54 Å). The average crystallite sizes, which are approximately the average particle sizes of the DNDs, were then calculated using Scherrer's formula based on the (111) diffraction peak showing the strongest diffraction intensities. Transmission electron microscopy (TEM) (JEOL, JEM-1400 plus, acceleration voltage 120 kV) was performed on a few droplets of the water-suspended DNDs dried under ambient conditions on a grid. The air-oxidized samples were characterized by PL spectroscopy using a Raman spectrometer

(HORIBA, Lab RAM Evolution) equipped with a narrow linewidth laser with an excitation wavelength of 532 nm.

The isolation of single-digit nanometer-sized DNDs was carried out via the following procedure. A colloidal solution was prepared from 12 mg of the air-oxidized DNDs with 8 mL of DI water followed by the sonication using an ultrasound horn (Hielscher Ultrasonics, UP-400S) at 120 W for 1 h to ensure a proper dispersion. The dispersion was then centrifuged (Hitachi Koki, CR22G) at 13,200 ×g for 1 h. The supernatant (up to 4 mm deep from the liquid level) was collected carefully using a micropipette. After the separated supernatant was dried, PL spectroscopy was performed by the method described above. A similar procedure for the isolation of single-digit nanometer-sized DNDs is demonstrated in reference [41].
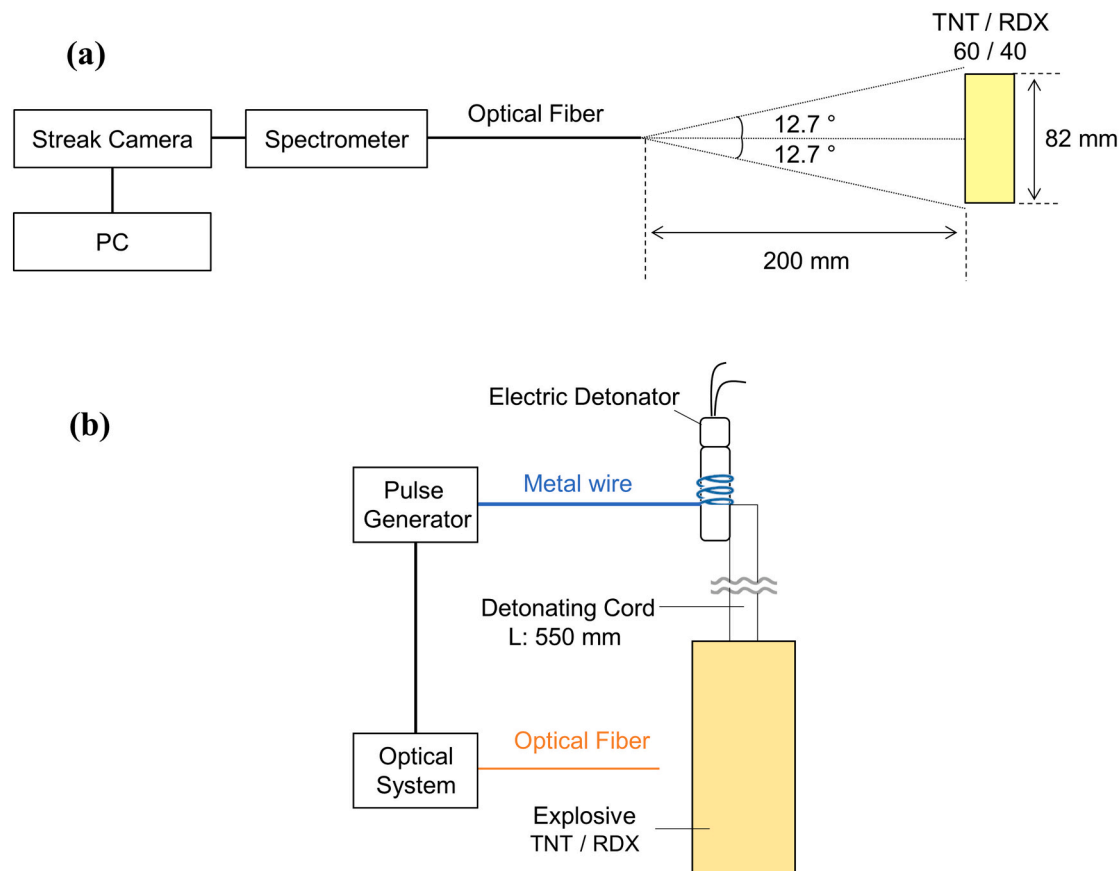

Fig. 3. (a) Schematic of the optical system. The distance between the explosive and the optical fiber end was set to 200 mm, as calculated by the height of the explosive (82 mm) and the numerical aperture of the optical fiber (12.7°). (b) Schematic of the overall experimental setup for the time-resolved optical emission measurements of the detonation phenomena.

In the optical measurement of the detonation phenomena to consider the key factors why SiV-DNDs were successfully synthesized only when TPS was used, each explosive (TR-explosive and two types of Si-explosives containing 6 g of each dopant) was detonated in air atmosphere and the emitted light collected through an optical fiber was detected by a streak camera (Hamamatsu Photonics, C2830) with a spectrometer (Hamamatsu Photonics, C5094). It should be mentioned here that, for the purpose of clearer observation of dopant-attributed light emission, the amounts of each dopant for the optical measurement were increased ten times as compared to the ones used for the SiV-DNDs synthesis. As schematically shown in Fig. 3, the optical fiber was positioned where the entire explosive could be captured. Using this optical system, the time-resolved spectra were recorded with the time and spectral resolution of 130 ns and 0.4 nm, respectively. It should be noted here that both the wavelength and intensity were calibrated using a mercury-argon lamp and a standard tungsten lamp. The streak camera was triggered by the ignition of the electric detonator with a metal wire. This is a widely-used trigger-signal generation method for the measurement of detonation phenomena [42]. On the other hand, the explosive was ignited by the electric detonator through the detonating cord. The difference in transmission time between the metal wire and the detonating cord was eliminated by adjusting the length of the detonating cord. This method enables to synchronize the activation of the streak camera with the ignition of the explosive.

3. Results and discussion

The XRD patterns of the purified detonation products obtained from the two types of Si-explosives are shown in Fig. 4. The products were confirmed to have a diamond crystal structure as three major diffraction peaks, originated from (111), (220), and (311) planes, were clearly observed. Peaks of graphite were not observed. The average particle sizes of the DNDs obtained from TPS (DNDs-TPS) and TTS (DNDs-TTS) calculated based on each (111) diffraction peak using Scherrer's formula were 7.1 and 7.4 nm, respectively. Meanwhile, TEM images of the aggregated DNDs-TPS and DNDs-TTS are shown in Fig. 5a and b, respectively, and the histograms of the particle size distributions estimated from these images were presented in Fig. 5c and d, respectively. These indicate that both DNDs-TPS and DNDs-TTS have primary particle sizes of about 7 nm, meaning that single-digit nanometer-sized DNDs were produced for both Si-explosives.

The measurements of PL spectra on the obtained DNDs were performed and the intensities of PL at 738 nm are mapped Fig. 6a and b. As can be seen in Fig. 6a, DNDs-TPS exhibit many bright spots (e.g., spot 1 in Fig. 6a). However, no significant bright spots are observed for the DNDs-TTS (Fig. 6b). In Fig. 6c, the representative PL spectra for DNDs-TPS and DNDs-TTS (spots 1 and 2 indicated in Fig. 6a and b, respectively) are shown. One can clearly see that only DNDs-TPS has a distinct

peak centered at 738 nm. This peak position has an agreement with the well-known wavelength of ZPL for the SiV center, suggesting that SiV-center containing single-digit NDs were successfully synthesized via the detonation process using the explosive containing TPS as a silicon source. It should be mentioned here that the density of the SiV centers in the DNDs was estimated to be at least 2×10^{13} to 2×10^{14} cm^{-3} through the analysis of confocal fluorescence images (stated in detail in Supplementary data, Section 1).

It is known that a typical PL spectrum of SiV centers is composed of a prominent ZPL and weak sidebands [43]. In our case of the SiV centers in DNDs-TPS, the PL spectrum can be well-fitted with two Lorentzian curves: one is the sharp peak centered at 738.4 nm and the other is broadband centered at 755.2 nm (see Fig. 6d), which are assigned to the ZPL and sideband, respectively. Here, according to Lindner et al. [43], SiV centers in NDs could be separated into two groups depending on the center wavelength and linewidth of the ZPL emission. The first group is defined when the center wavelength and linewidth of the ZPL are ranging from 730 to 742 nm and from 5 to 17 nm, respectively. As an additional characteristic for the first group, most of the SiV centers display a wavelength shift of the sidebands from the ZPL ranging from 37 to 43 meV. Such SiV centers are expected to have a well-known SiV structure like the one shown in Fig. 1. In contrast, the SiV centers enclosed in the second group exhibit a ZPL with a broad distribution of a center wavelength (ranging from 715 to 835 nm) and a narrow linewidth (usually below 1–4 nm). Such SiV centers are considered to have an unclear/undefined structure composed of any fluorescent defects containing silicon. In our case of DNDs-TPS, the ZPL's center wavelength and linewidth are 738.4 nm and 16.6 nm, respectively, and the wavelength shift of sideband's peak top from the ZPL is 37.4 meV (16.8 nm). Namely, the SiV centers in DNDs-TPS belong to the first group, presumably including that they have the typical SiV structure.

To confirm that SiV centers are contained in the single-digit nanometer-sized DNDs-TPS as well as the aggregates and minor larger (> 10 nm) particles, we explored to isolate the single-digit nanometer-sized DND particles. As stated in Chapter 2, the air-oxidized DNDs-TPS were ultrasonicated and then centrifuged (13,200 $\times g$, 1 h). After the centrifugation, the supernatant (up to 4 mm deep from the liquid level) was collected. Here, the sedimentation velocity V_{sed} of the particle in a solvent is generally given by [44]:

$$V_{sed} = \frac{2gr^2(\rho_p - \rho_s)}{9\eta}, \tag{1}$$

where g is the gravitational acceleration, r is the radius of the particle, $(\rho_p - \rho_s)$ is the density difference between the particle and the solvent, and η is the viscosity of the solvent. In the case of present system, when the DNDs of > 10 nm are centrifuged at 13,200 $\times g$, the sedimentation velocity is calculated to be > 6.4 mm/h via Eq. (1). Therefore, the

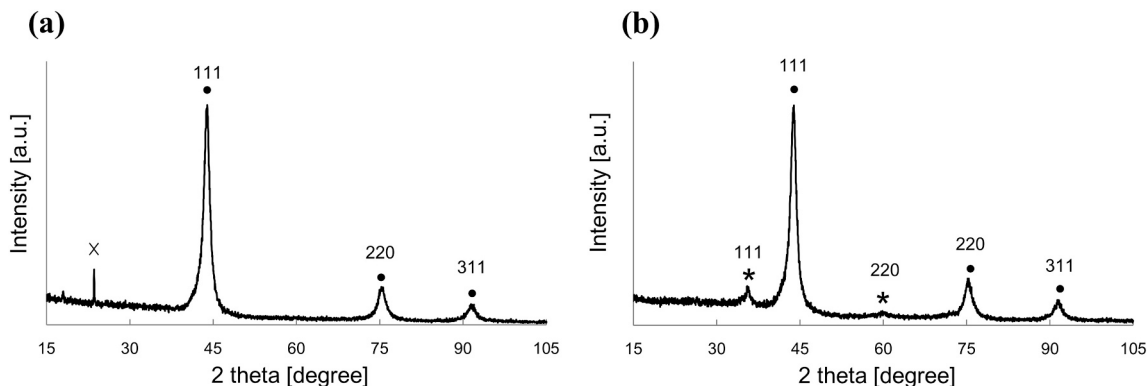**(a)**   **(b)**

Fig. 4. XRD patterns of the detonation products obtained from the two types of Si-explosives: (a) TPS and (b) TTS. The dots indicate a cubic diamond structure, and the asterisks denote cubic silicon carbide. The cross indicates a spike noise.
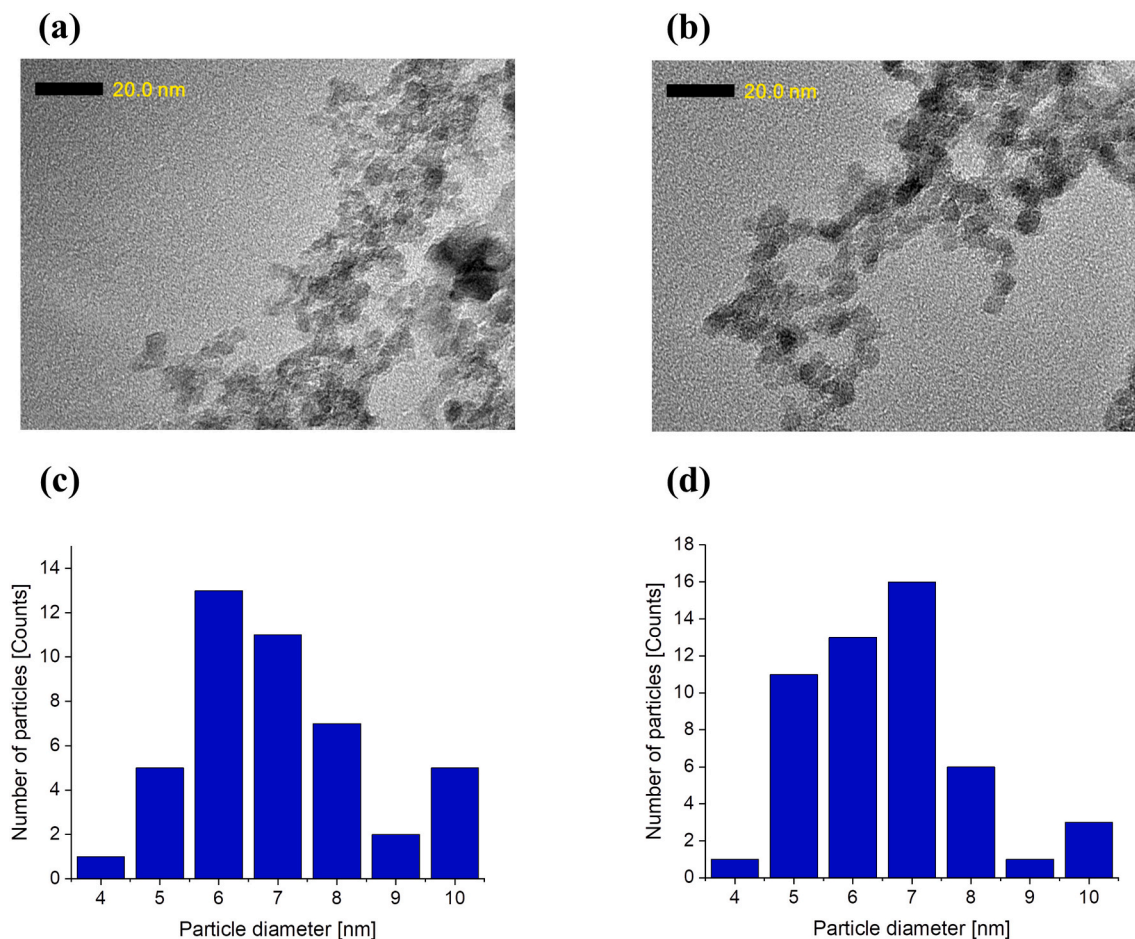
(a)

(b)

(c)

(d)

Fig. 5. TEM images of aggregated (a) DNDs-TPS and (b) DNDs-TTS particles. Histograms of the particle size distribution of (c) DNDs-TPS and (d) DNDs-TTS obtained from the TEM images. The NDs with particle sizes over 10 nm, which are hardly recognized from the strongly aggregated NDs' TEM images, might be included in the detonation products. However, such NDs should not critically affect the particle size distributions because only a few of them can be found in the images.

collected supernatant (up to 4 mm deep from the level) should contain only single-digit nanometer-sized DNDs. As shown in Fig. 7, such DNDs-TPS exhibited a PL peak attributed to the SiV center, surely indicating that single-digit nanometer-sized SiV-DNDs were obtained. Notice that the linewidth of ZPL (18.6 nm) was slightly wider than that of the SiV-DNDs before the isolation treatment (16.6 nm, see Fig. 6d). Thus, the SiV structures in DNDs of smaller size are presumed to be marginally distorted than the ones in larger DNDs due to the extremely small size [45]. Here, the formation of color centers such as SiV in diamond sometimes requires annealing to mobilize vacancies and facilitate their connection with heteroatoms such as silicon atoms [46]. However, in the case of present study, SiV centers were directly formed in DNDs without any post-treatment like annealing. Similarly, nanometer-sized or bulk diamonds containing SiV centers were synthesized by HPHT and CVD methods without annealing [34,47]. Certainly, it is widely known that SiV centers are energetically more stable than Si-substitutional defects within the diamond lattice [48–50] and, therefore, could be more preferentially formed under the environment of diamond formation.

To investigate the key factors why SiV-DNDs were fabricated only when using TPS as silicon source, we observed temporal evolution of the detonation from TR- and Si-explosives containing 6 g each dopant using time-resolved optical emission spectroscopy. The time-resolved spectra of the emission from the detonation reactions are shown in Fig. 8a–c. Fig. 8a'–c' show the spectra extracted by the integration for 13 μs after the start of the significant emission (e.g., 10 to 23 μs in Fig. 8a), which is the same time-domain as the appearance of the detonation observed with a high-speed camera (see Supplementary data, Section 2). These

spectra could not be fitted with a Planck distribution and showed several sharp peaks at 422, 588, 768, and 819 nm. These peaks are attributable to emission from the detonation reaction. In addition to these, a special peak was observed at 670 nm when using TTS. These peaks at 422, 588 and 670 nm were assigned to O(II) [$2s^22p^2(^3P)3d$–$2s^22p^2(^3P)4f$], C(I) [$2s^22p3p$–$2s^22p7s$] and Si(IV) [$2p^65p$–$2p^65d$] atomic emissions [51], respectively, from high-resolution experimental data using a finer grating (spectral resolution: 0.04 nm). These time-resolved spectra did not show Swan-bands of C_2, which are characteristic of the radical of diatomic carbon (C_2) [52–54]. The absence of these bands indicates that C_2 is not a major component in the DND formation process. However, because molecular species cannot be observed in this experiment, there is also room for consideration that molecular species larger than C_3 are involved in the DND formation.

Here, the DND formation mechanism is discussed. According to Danilenko, the basic mechanism of DND formation is that the self-decomposed explosive carbon species condense and crystallize via droplets in the high-temperature and high-pressure environment of the detonation (behind the C-J plane), in agreement with the nanoscale carbon phase diagram [55]. This hypothesis is widely accepted [1,2]. Dolmatov summarized that the role of RDX is to create a sufficiently high pressure and temperature to enable the liquid-to-diamond phase transition, whereas TNT is the carbon source of the DNDs. This statement was deduced from isotope experiments and investigations of the relationship between the amount of TNT in explosives and the yield of DNDs [56,57]. Rom et al. simulated the decomposition process of 288 TNT molecules under a high temperature and high pressure using
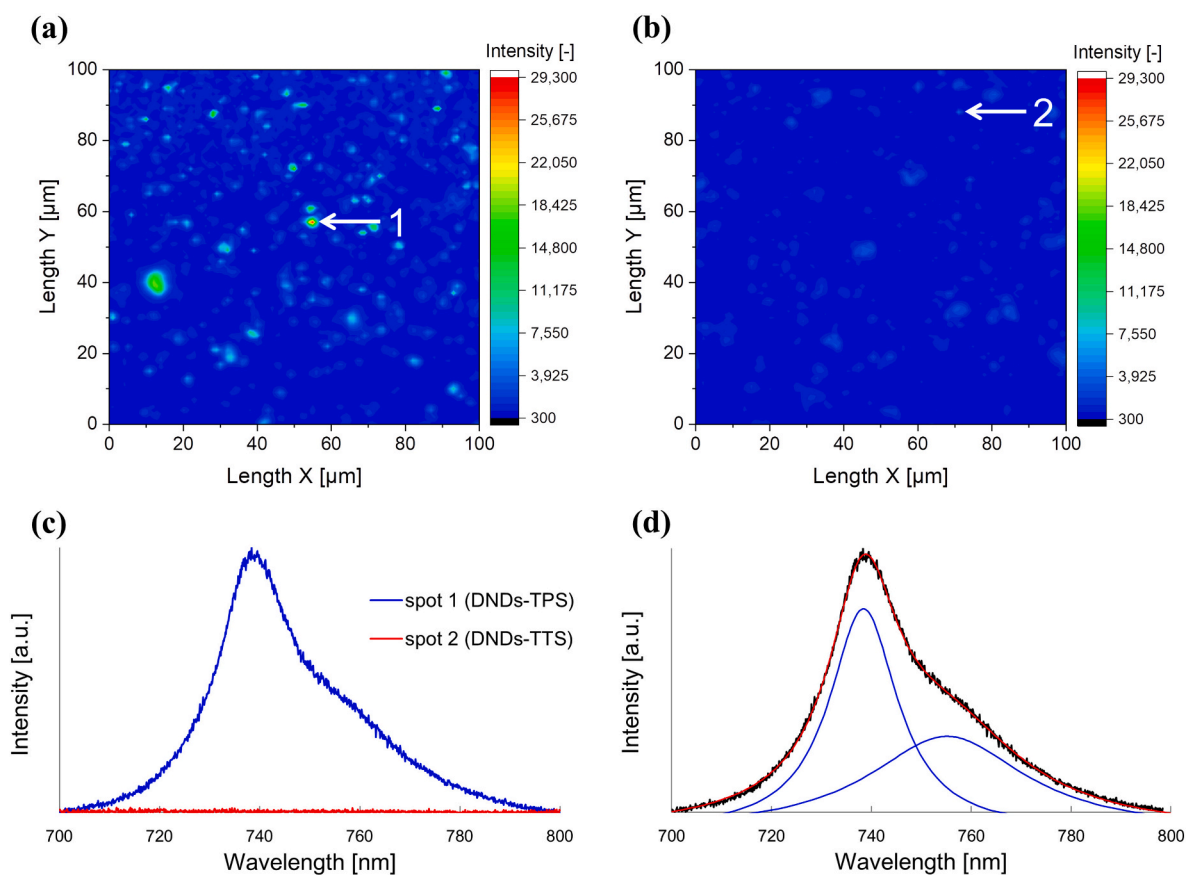
Fig. 6. The results of PL measurements on a SiV color center in DND using a Raman spectroscopy system. The intensity mapping of PL at 738 nm for (a) DNDs-TPS and (b) DNDs-TTS. (c) The PL spectra corresponding to the spots 1 and 2 indicated in (a, b). (d) Lorentzian fitting curves (two blue line curves) for the PL spectrum on the spot 1. The red and black curves indicate the fitted curve and the original spectrum, respectively. (For interpretation of the references to color in this figure legend, the reader is referred to the web version of this article.)
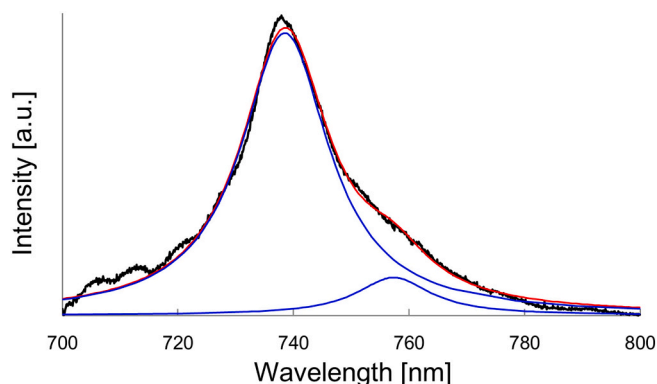

Fig. 7. A PL spectrum of the separated single-digit nanometer-sized DNDs-TPS and Lorentzian fitting curves (two blue line curves) for the PL spectrum. The red and black curves indicate the fitted curve and the original spectrum, respectively. The center wavelength of the ZPL and sideband are 738.5 nm and 757.3 nm, respectively. The wavelength shift of sideband's peak top from the ZPL is 41.7 meV (18.8 nm). The linewidth of the ZPL is 18.6 nm. (For interpretation of the references to color in this figure legend, the reader is referred to the web version of this article.)

LAMMPS-ReaxFF [58]. They found that the initial decomposition begins with C–N bond scissions, followed by the formation of TNT dimers, meaning that the carbon cluster formation proceeds while the six-membered ring structure of TNT (C_6) is maintained. Combining these findings with the results of our optical experiments, we propose that, although atomic carbon observed in optical experiments may be involved in diamond formation, C_6 molecular species from TNT is likely the main building block for DND formation. We thereby consider that TNTs couple and aggregate with themselves while maintaining the C_6-structure, and undergoes a phase transition from the liquid phase to the diamond phase during the detonation reaction (hereinafter referred to as the C_6-mechanism).

C_6-mechanism enables us to interpret the reason why the SiV-DND was synthesized only when using TPS as silicon source. The spectra of Si-explosives with TTS indicate atomic emission of Si while, those with TPS do not. These results suggest that TTS is decomposed into atoms and TPS maintained the chemical structure in whole either in part in the detonation reaction. Importantly, TPS consists of the same six-membered ring structure (C_6) as TNT. Considering these, therefore, we suggest that some interactions combine TPS and the DND building blocks while C_6 structures were maintained and, as a result, Si atoms were incorporated into the diamond crystal lattice.

4. Conclusions

In this study, we succeeded in fabricating single-digit nanometer-sized DNDs containing SiV centers via detonation process using TPS as a silicon source. In addition, the discussion of DND formation mechanism based on the time-resolved optical emission spectroscopy revealed that the factor of this success may be attributed to the aromatic ring of TPS. The achievement of synthesizing SiV-NDs of single-digit nanometer size by the detonation processes, which is the most productive manufacturing method of NDs, will dramatically advance the field of bioimaging/sensing. Moreover, we expect this study to be extended to
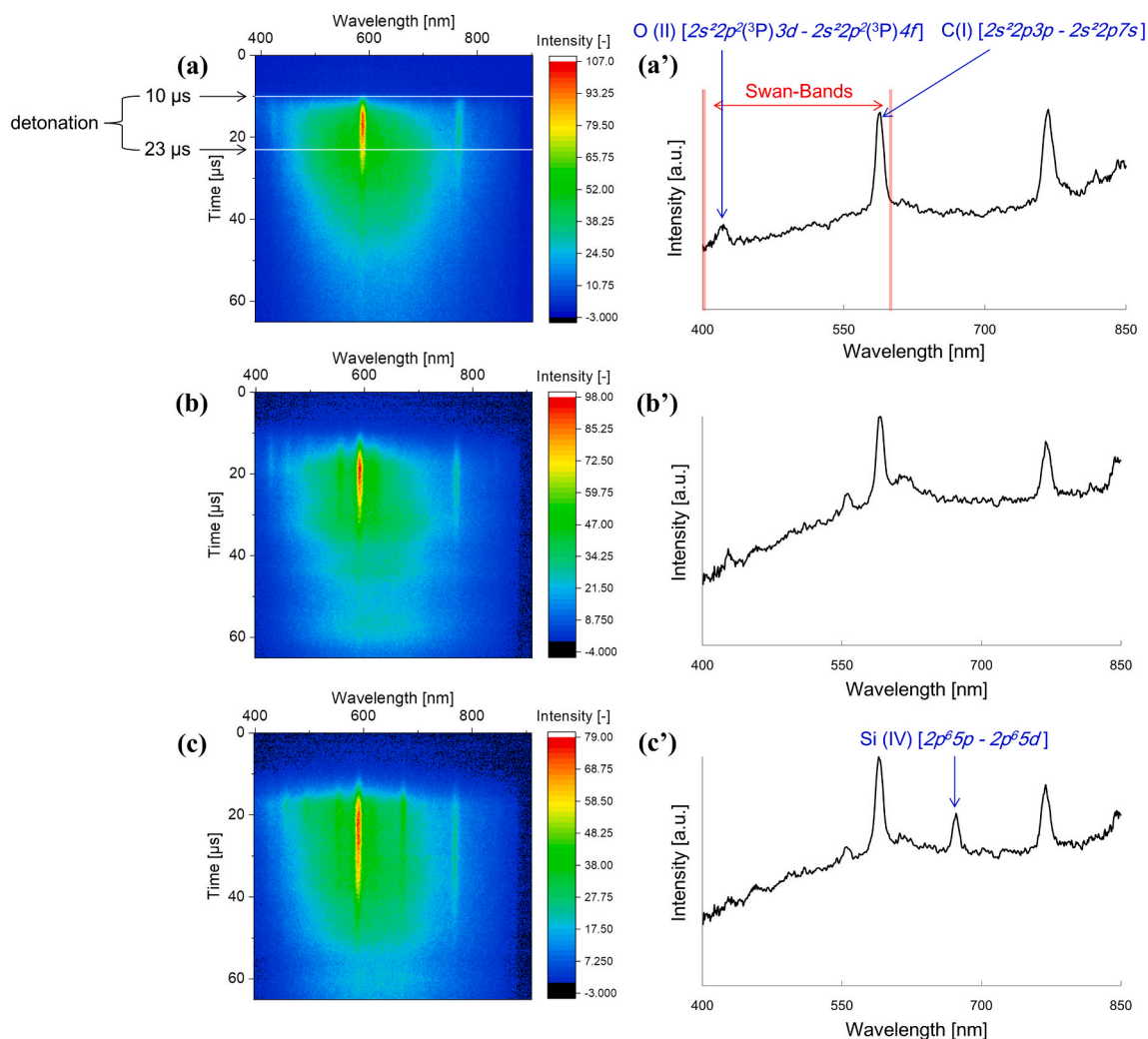
Fig. 8. The two-dimensional plots of the time-resolved spectra of the emission from (a) TR-explosive and two types of Si-explosives including (b) TPS and (c) TTS. In all cases, detonation phenomena occurred for about 13 μs and a secondary combustion was observed after detonation reaction. Time-integrated spectra of the detonation using (a') TR-explosive and two Si-explosives including (b') TPS and (c') TTS.

the development of any heteroatom doping technology for the synthesis of NDs.

CRediT authorship contribution statement

Yuto Makino: Conceptualization, Methodology, Validation, Formal analysis, Investigation, Data curation, Writing - Original Draft, Visualization.

Tomoaki Mahiko: Conceptualization, Validation, Investigation, Writing - Review & Editing, Project administration.

Ming Liu: Validation, Investigation.

Akihiko Tsurui: Validation, Investigation.

Taro Yoshikawa: Validation, Investigation, Formal analysis, Writing - Review & Editing.

Shinji Nagamachi: Validation, Formal analysis, Investigation.

Shigeru Tanaka: Methodology, Validation, Investigation.

Kazuyuki Hokamoto: Methodology, Validation, Resource, Project administration.

Masaaki Ashida: Methodology, Validation, Formal analysis,

Investigation, Resource, Supervision, Project administration.

Masanori Fujiwara: Methodology, Validation, Formal analysis, Investigation.

Norikazu Mizuochi: Methodology, Validation, Formal analysis, Resource, Project administration.

Masahiro Nishikawa: Validation, Resource, Writing - Review & Editing, Supervision.

Declaration of competing interest

The authors declare that they have no known competing financial interests or personal relationships that could have appeared to influence the work reported in this paper.

Appendix A. Supplementary data

Supplementary data to this article can be found online at https://doi.org/10.1016/j.diamond.2021.108248.

References

[1] J.-C. Arnault, Nanodiamonds: advanced material analysis, properties and applications, 1st ed., Elsevier, Amsterdam, 2017, pp. 166–172, pp. xix, 25–31.
[2] V.N. Mochalin, O. Shenderova, D. Ho, Y. Gogotsi, The properties and applications of nanodiamond, Nat. Nanotechnol. 7 (2012) 11–23.

[3] V.V. Danilenko, Nanodiamond: problems and prospects, Journal of Superhard materials 32 (2010) 301–310.

[4] N. Nunn, O. Shenderova, Toward a golden standard in single digit detonation nanodiamond, Phys. Status Solid A 213 (2016) 2138–2145.

[5] L. Schmidlin, V. Pichot, M. Comet, S. Josset, P. Rabu, D. Spitzer, Identification, quantification and modification of detonation nanodiamond functional groups, Diam. Relat. Mater. 22 (2012) 113–117.

[6] T. Jiang, K. Xu, FTIR study of ultradispersed diamond powder synthesized by explosive detonation, Carbon 33 (1995) 1663–1671.

[7] M.S. Shestakov, S.P. Vul, A.T. Dideikin, T.V. Larionova, A.V. Shvidchenko, E. B. Yudina, V.V. Shnitov, Advanced oxidation process for detonation nanodiamond surface chemical modification, J. Phys. Conf. Ser. 1400 (2019), 055044.

[8] W.S. Yeap, S. Chen, K.P. Loh, Detonation nanodiamond: an organic platform for the Suzuki coupling of organic molecules, Langmuir 25 (2009) 185–191.

[9] V.N. Mochalin, Y. Gogotsi, Nanodiamond-polymer composites, Diam. Relat. Mater. 58 (2015) 161–171.

[10] X.-B. Cheng, M.-Q. Zhao, C. Chen, A. Pentecost, K. Maleski, T. Mathis, X.-Q. Zhang, Q. Zhang, J. Jiang, Y. Gogotsi, Nanodiamonds suppress the growth of lithium dendrites, Nat. Commun. 8 (2017) 336.

[11] A.V. Shvidchenko, E.D. Eidelman, A.Ya. Vul, N.M. Kuznetsov, D. Yu, S.I. Belousov Stolyarova, S.N. Chvalun, Colloids of detonation nanodiamond particles for advanced applications, Adv. Colloid Interface Sci. 268 (2019) 64–81.

[12] I. Petrov, P. Detkov, A. Drovosekov, M.V. Ivanov, T. Tyler, O. Shenderova, N. P. Voznecova, Y.P. Toporov, D. Schulz, Nickel galvanic coatings co-deposited with fractions of detonation nanodiamond, Diam. Relat. Mater. 15 (2006) 2035–2038.

[13] A. Kruger, New carbon materials: biological applications of functionalized nanodiamond materials, Chem. Eur. J. 14 (2008) 1382–1390.

[14] J.M. Say, C. van Vreden, D.J. Reilly, L.J. Brown, J.R. Rabeau, N.J. King, Luminescent nanodiamonds for biomedical applications, Biophys. Rev. 3 (2011) 171–184.

[15] V. Pichot, O. Stephan, M. Comet, E. Fousson, J. Mory, K. March, D. Spitzer, High nitrogen doping of detonation nanodiamonds, J. Phys. Chem. C 114 (2010) 10082–10087.

[16] A. Krüger, Y. Liang, G. Jarre, J. Stegk, Surface functionalization of detonation diamond suitable for biological applications, J. Mater. Chem. 16 (2006) 2322–2328.

[17] L. Zhao, Y.-H. Xu, T. Akasaka, S. Abe, N. Komatsu, F. Watari, X. Chen, Polyglycerol-coated nanodiamond as a macrophage-evading platform for selective drug delivery in cancer cells, Biomaterials 35 (2014) 5393–5406.

[18] H. Huang, E. Pierstorff, E. Osawa, D. Ho, Active nanodiamond hydrogels for chemotherapeutic delivery, Nano Lett. 7 (2017) 3305–3314.

[19] M. Chen, X.-Q. Zhang, H.B. Man, R. Lam, E.K. Chow, D. Ho, Nanodiamond vectors functionalized with polyethylenimine for siRNA delivery, J. Phys. Chem. Lett. 1 (2010) 3167–3171.

[20] V.N. Mochalin, Y. Gogotsi, Wet chemistry route to hydrophobic blue fluorescent nanodiamond, J. Am. Chem. Soc. 131 (2009) 4594–4595.

[21] Z. Wang, C.X. Xu, C. Liu, Surface modification and intrinsic green fluorescence emission of a detonation nanodiamond, J. Mater. Chem. C 1 (2013) 6630–6636.

[22] S.L.Y. Chang, A.S. Barnard, C. Dwyer, C.B. Boothroyd, R.K. Hocking, E. Ōsawa, R. J. Nicholls, Counting vacancies and nitrogen-vacancy centers in detonation nanodiamond, Nanoscale 8 (2016) 10548–10552.

[23] C. Bradac, T. Gaebel, N. Naidoo, M.J. Sellars, J. Twamley, L.J. Brown, A.S. Barnard, T. Plakhotnik, A.V. Zvyagin, J.R. Rabeau, Observation and control of blinking nitrogen-vacancy centres in discrete nanodiamonds, Nat. Nanotech. 5 (2010) 345–349.

[24] P. Reineck, M. Capelli, D.W.M. Lau, J. Jeske, M.R. Field, T. Ohshima, A. D. Greentreea, B.C. Gibson, Bright and photostable nitrogen-vacancy fluorescence from unprocessed detonation nanodiamond, Nanoscale 9 (2017) 497–502.

[25] V.Yu. Osipov, S.A. Zargaleh, F. Treussart, K. Takai, N.M. Romanov, F.M. Shakhov, A. Baldycheva, Nitrogen impurities and fluorescent nitrogen-vacancy centers in detonation nanodiamonds: identification and distinct features, J. Opt. Technol. 86 (2019) 1–8.

[26] E. Neu, C. Arend, E. Gross, F. Guldner, C. Hepp, D. Steinmtz, E. Zscherpel, S. Ghodbane, H. Sternschulte, D. Steinmüller-Nethl, Y. Liang, A. Kruger, C. Becher, Narrowband fluorescent nanodiamonds produced from chemical vapor deposition films, App. Phys. Lett. 98 (2011) 243107.

[27] A.M. Smith, M.C. Mancini, S. Nie, Second window for *in vivo* imaging, Nat. Nanotech. 4 (2009) 710–7111.

[28] V. Vaijayanthimala, P.-Y. Cheng, S.-H. Yeh, K.-K. Liu, C.-H. Hsiao, J.-I. Chao, H. C. Chang, The long-term stability and biocompatibility of fluorescent nanodiamond as an in vivo contrast agent, Biomaterials 33 (2012) 7794–7802.

[29] E. Neu, F. Guldner, C. Arend, Y. Liang, S. Ghodbane, H. Sternschulte, D. Steinmüller-Nethl, A. Kruger, C. Becher, Low temperature investigations and surface treatments of colloidal narrowband fluorescent nanodiamonds, J. App. Phys. 113 (2013) 203507.

[30] R. Weissleder, A clear vision for *in vivo* imaging: Progress continues in the development of smaller, more penetrable probes for biological imaging, Nat. Biotechnol. 19 (2001) 316–317.

[31] A.M. Zaitsev, Vibronic spectra of impurity-related optical centers in diamond, Phys. Rev. B 61 (2000) 12909–12922.

[32] L.J. Rogers, K.D. Jahnke, M.W. Doherty, A. Dietrich, L.P. McGuinness, C. Müller, T. Teraji, H. Sumiya, J. Isoya, N.B. Manson, F. Jelezko, Electronic structure of the negatively charged silicon-vacancy center in diamond, Phys. Rev. B 89 (2014) 235101.

[33] Y. Mei, C. Chen, D. Fan, M. Jiang, X. Li, X. Hu, Enhanced SiV photoluminescence by oxidation-induced nano-structures on diamond particle surface, Nanoscale 11 (2019) 656–662.

[34] S.V. Bolshedvorskii, A.I. Zeleneev, V.V. Vorobyov, V.V. Soshenko, O.R. Rubinas, L. A. Zhulikov, P.A. Pivovarov, V.N. Sorokin, A.N. Smolyaninov, L.F. Kulikova, A. S. Garanina, S.G. Lyapin, V.N. Agafonov, R.E. Uzbekov, V.A. Davydov, A. V. Akimov, Single silicon vacancy centers in 10 nm diamonds for quantum information applications, ACS Appl. Nano Mater. 2 (2019) 4765–4772.

[35] S. Häußler, G. Thiering, A. Dietrich, N. Waasem, T. Teraji, J. Isoya, T. Iwasaki, M. Hatano, F. Jelezko, A. Gali, A. Kubanek, Photoluminescence excitation spectroscopy of SiV⁻ and GeV⁻ color center in diamond, New J. Phys. 19 (2017), 063036.

[36] V.A. Shershulin, V.S. Sedov, A. Ermakova, U. Jantzen, L. Rogers, A.A. Huhlina, E. G. Teverovskaya, V.G. Ralchenko, F. Jelezko, I.I. Vlasov, Size-dependent luminescence of color centers in composite nanodiamonds, Phys. Status Solidi A 212 (2015) 2600–2605.

[37] I.I. Vlasov, A.A. Shiryaev, T. Rendler, S. Steinert, S.-Y. Lee, D. Antonov, M. Vörös, F. Jelezko, A.V. Fisenko, L.F. Semjonova, J. Biskupek, U. Kaiser, O.I. Lebedev, I. Sildos, P.R. Hemmer, V.I. Konov, A. Gali, J. Wrachtrup, Molecular-sized fluorescent nanodiamonds, Nat. Nanotechnol. 9 (2014) 54–58.

[38] S. Heyer, W. Janssen, S. Turner, Y.-G. Lu, W.S. Yeap, J. Verbeeck, K. Haenen, A. Kruger, Toward deep blue nano hope diamonds: heavily boron-doped diamond nanoparticles, ACS Nano 8 (2014) 5757–5764.

[39] A.G. Brook, S. Wolfe, The reaction of triphenylsilylpotassium with organic halides, a case of halogen-metal interconversion, J. Am. Chem. Soc. 79 (1957) 1431–1437.

[40] M. Ishikawa, J. Iyoda, H. Ikeda, K. Kotake, T. Hashimoto, M. Kumada, Aluminum chloride catalyzed skeletal rearrangement of permethylated acyclic polysilanes, J. Am. Chem. Soc. 103 (1981) 4845–4850.

[41] S. Stehlik, M. Varga, M. Ledinsky, D. Miliaieva, H. Kozak, V. Skakalova, C. Mangler, T.J. Pennycook, J.C. Meyer, A. Kromka, B. Rezek, High-yield fabrication and properties of 1.4 nm nanodiamonds with narrow size distribution, Sci. Rep. 6 (2016) 38419.

[42] S. Tanaka, I. Bataev, M. Nishi, I. Balagansky, K. Hokamoto, Micropunching large-area metal sheets using underwater shock wave: experimental study and numerical simulation, Int. J. Mach. Tools Manuf. 147 (2019) 103457.

[43] S. Lindner, A. Bommer, A. Muzha, A. Krueger, L. Gines, S. Mandal, O. Williams, E. Londero, A. Gali, C. Becher, Strongly inhomogeneous distribution of spectral properties of silicon-vacancy color centers in nanodiamonds, New J. Phys. 20 (2018) 115002.

[44] R.M. Pashley, M.E. Karaman, Applied Colloid and Surface Chemistry, John Wiley & Sons, Ltd., New York, 2004, pp. 1–6.

[45] U. Jantzen, A.B. Kurz, D.S. Rudnicki, C. Schäfermeier, K.D. Jahnke, U.L. Andersen, V.A. Davydov, V.N. Agafonov, A. Kubanek, L.J. Rogers, F, Jelezko, Nanodiamonds carrying silicon-vacancy quantum emitters with almost lifetime-limited linewidths, New J. Phys. 18 (2016), 073036.

[46] R.E. Evans, A. Sipahigil, D.D. Sukachev, A.S. Zibrov, M.D. Lukin, Narrow-linewidth homogeneous optical emitters in diamond nanostructures via silicon ion implantation, Phys. Rev. Applied. 5 (2016), 044010.

[47] A. Bolshakov, V. Ralchenko, V. Sedov, A. Khomich, I. Vlasov, A. Khomich, N. Trofimov, V. Krivobok, S. Nikolaev, R. Khmelnitskii, V. Saraykin, Photoluminescence of SiV centers in single crystal CVD diamond in situ doped with Si from silane, Phys. Status Solidi A 212 (2015) 2525–2532.

[48] A.M. Edmonds, M.E. Newton, P.M. Martineau, D.J. Twitchen, S.D. Williams, Electron paramagnetic resonance studies of silicon-related defects in diamond, Phys. Rev. B 77 (2008) 245205.

[49] J.P. Goss, P.R. Briddon, M.J. Rayson, S.J. Sque, R. Jones, Vacancy-impurity complexes and limitations for implantation doping of diamond, Phys. Rev. B 72 (2005), 035214.

[50] A.S. Barnard, I.I. Vlasov, V.G. Ralchenko, Predicting the distribution and stability of photoactive defect centers in nanodiamond biomarkers, J. Mater. Chem. 19 (2009) 360–365.

[51] A. Kramida, Yu. Ralchenko, J. Reader, NIST ASD Team (2019). NIST atomic spectra database (version 5.7.1), [Online]. Available: https://physics.nist.gov/asd [Tue Mar 31 2020]. National Institute of Standards and Technology, Gaithersburg, MD. DOI: 10.18434/T4W30F.

[52] A.G. Gaydon, The spectroscopy of Flame, 2nd ed., Chapman and Hall, London, 1974, pp.146–147, 343.

[53] J.E.M. Goldsmith, D.T.B. Kearsley, C₂ creation, emission, and laser-induced fluorescence in flames and cold gases, App. Phys. B 50 (1990) 371–379.

[54] D. Amans, A.-C. Chenu, G. Ledoux, C. Dujardin, C. Reynaud, O. Sublemontier, K. Masenelli-Varlot, O. Guillois, Nanodiamond synthesis by pulsed laser ablation in liquids, Diam. Relat. Mater. 18 (2009) 177–180.

[55] V.V. Danilenko, Specific features of synthesis of detonation nanodiamonds, Combustion, explosion, and shock waves 41 (2005) 577–588.

[56] V.Yu. Dolmatov, V. Myllymäki, A. Vehanen, A possible mechanism of nanodiamond fromation during detonation synthesis, J. Superhard Mater. 35 (2013) 143–150.

[57] V.Yu. Dolmatov, On the mechanism of detonation nanodiamond synthesis, J. Superhard Mater. 30 (2008) 233–240.

[58] N. Rom, B. Hirshberg, Y. Zeiri, D. Furman, S.V. Zybin, W.A. Goddard III, R. Kosloff, First-principles-based reaction kinetics for decomposition of hot, dense liquid TNT from ReaxFF multiscale reactive dynamics simulations, J. Phys. Chem. C 117 (2013) 21043–21054.